Frontotemporal network engagement by human intracranial stimulation in limbic hubs

Anusha Allawala[1,2], Kelly R Bijanki[3], Denise Oswalt[4], Raissa K Mathura[3], Joshua Adkinson[3], Victoria Pirtle[3], Brian Metzger[5], Ben Shofty[6], Meghan Robinson[3], Adrish Anand[3], Ricardo A Najera[3], Ron Gadot[3], Matthew T Harrison[7], Sanjay J Mathew[8], Wayne K Goodman[8], Nader Pouratian[9], Sameer A Sheth[3]*, David A Borton[1,2,10]*†

Affiliations:

1 School of Engineering, Brown University, Providence, RI, United States

2 Carney Institute for Brain Science, Providence, RI, United States

3 Department of Neurosurgery, Baylor College of Medicine, Houston, TX, United States

4 Department of Neurosurgery, University of Pennsylvania, Philadelphia, PA, United States

5 Department of Psychology, Swarthmore College, Swarthmore, PA, United States

6 Department of Neurosurgery, University of Utah, Salt Lake City, UT, United States

7 Division of Applied Mathematics, Brown University, Providence, RI, United States

8 Menninger Department of Psychiatry and Behavioral Sciences, Baylor College of Medicine, Houston, TX, United States

9 Department of Neurological Surgery, UT Southwestern Medical Center, Dallas, TX, United States

10 Department of Veterans Affairs, Center for Neurorestoration and Neurotechnology, Providence, RI, United States

*denotes equal contribution

† denotes corresponding author: david_borton@brown.edu

Abstract

Frontotemporal circuits in the human brain play an important role in cognitive and affective processing. Neuromodulation therapies delivered to certain key hubs within these circuits are being used with increasing frequency to treat a host of neuropsychiatric disorders, but the detailed neurophysiological effects of stimulation are largely unknown. Here, we performed intracranial recordings across frontotemporal networks while delivering electrical stimulation to two well-established white matter hubs involved in cognitive regulation. We demonstrate a frontotemporal circuit consisting of the amygdala, lateral orbitofrontal cortex, and ventromedial prefrontal cortex in which gamma oscillations are differentially modulated depending on the target

stimulated. We additionally highlight the heterogeneity in neural responses to stimulation across human subjects in other corticolimbic regions and demonstrate the capacity for further tuning of neural activity using current-steered stimulation. Our findings indicate a potential neurophysiological mechanism for the dissociable therapeutic effects seen across targets for neuromodulation and implications for future efforts in personalized, network-guided neurostimulation.

Introduction

The abilities to regulate complex emotions and make controlled decisions are central to the human experience and critical for successful navigation through challenging life circumstances. Although these functions are broadly distributed across the brain, prefrontal and temporal regions play an especially important role in their regulation, as has been demonstrated by a number of neuroimaging and electrodiagnostic studies[1,2]. Frontotemporal networks have been demonstrated to subserve different functions in affective, cognitive, emotional and reward processing, and disruption of neural activity in these circuits produces disorders of mood, anxiety, impulsivity, apathy, and other related behavioral manifestations[3,4]. Causal manipulations of frontotemporal networks using electrical stimulation have provided further evidence of the close relationship between disrupted neural circuits and neuropsychiatric behavioral symptoms. Further, neuromodulation is commonly used to treat individuals with dysfunction in these circuits that manifests as treatment-resistant psychiatric disorders.

Examples of these neuromodulatory interventions include non-invasive methods such as transcranial magnetic stimulation (TMS)[5,6] and invasive ones such as deep brain stimulation (DBS)[7–9] and responsive neurostimulation (RNS)[10,11]. A critical feature of these interventions is that even though their delivery is highly focal – especially true for invasive techniques – their influence is quite broad. Neuroimaging and scalp EEG studies during therapeutic DBS in psychiatric indications, for example, have demonstrated its widespread effects across frontotemporal networks, despite the focal nature of its delivery[12–15]. Alterations in functional connectivity have been observed between nodes of these frontotemporal subnetworks following stimulation and have been linked to symptom improvement in mood disorders[13,16]. These changes in stimulation-driven connectivity raise the question about how best to target dysfunctional neural activity underlying affective disorders and utilize putative neural biomarkers of symptoms to drive effective neuromodulation therapy. If we

can improve our understanding of the specific spatiotemporal effects of therapeutic stimulation on neural activity across implicated frontotemporal networks, we can better predict how an individual might respond to neurostimulation. A broader understanding would subsequently drive more precise and targeted neuromodulation to treat symptoms in psychiatric disorders that arise from aberrant neural activity across frontotemporal circuits.

To engage frontotemporal networks of interest, stimulation is not required to be delivered to each node across the entire network, but instead can be delivered to “hubs” within well-connected circuits, in a data-driven manner, to enable predictable behavioral and electrophysiological output in response to neurostimulation. Due to the heterogeneity in affective, cognitive, and motor symptoms implicated in psychiatric disorders, and based on prior experience from lesioning surgeries, there are typically multiple candidate regions that can be targeted for neuromodulation therapy. The options for anatomical targeting are additionally accompanied by numerous choices of stimulation parameters and configurations. Therefore, quantitative characterization of the neural response to stimulation in frontotemporal circuits known to play multi-faceted roles in the processing of mood, affect and cognition is critical for the rational design of neuromodulation therapies to obtain the desired therapeutic outcome. Two well-characterized affective hubs, that have previously demonstrated to be gateways to parsimoniously engage larger networks in key frontotemporal and corticolimbic brain networks through invasive means[8,12,13,17], are the ventral capsule/ventral striatum (VC/VS) and subcallosal cingulate (SCC, also commonly referred to as Brodmann area 25 or Cg25).

It has been proposed that both the VC/VS and SCC are hubs at the crossroads of white matter pathways hypothesized to influence executive function[12], reward processing[18,19] and mood processing[8,20] through their connections of varying degrees to prefrontal and limbic structures (spanning the amygdala, prefrontal cortex, temporal cortex and cingulate cortex)[21,22] with partial overlap[23–25]. The “hub” hypothesis is supported by tractography and connectomic studies, where the SCC has been shown to project to the shell of the Nucleus Accumbens (NAc), suggesting “a point of convergence” between the two targets[26]. Additionally, targeting of the VC/VS and SCC has played an important role in both delivery of therapy and neural biomarker identification across a wide range of affective and cognitive behaviors and mood disorders. Modulation of the SCC has shown promising results in open-label DBS studies showing improvement in symptoms of anxiety[27]

and depression[8,28,29], treatment-refractory anorexia nervosa (AN)[30], and has been recently proposed as a target for chronic pain[31]. Similarly, the VC/VS has been successfully targeted for randomized controlled studies of DBS for obsessive-compulsive disorder (OCD)[32] as well as a host of smaller DBS studies for treatment-resistant depression (TRD)[20], addiction[33–35], refractory AN[36] and schizophrenia[37]. The SCC and VC/VS have also been implicated in reward processing[22,38], negative bias[39], affective processing[40] and emotion regulation[1,41]. It is therefore unsurprising that stimulation across the two regions have differential and broad effects on many of the behaviors across mental illnesses associated with disruption in activity in frontotemporal networks.

In the clinical treatment of TRD with DBS, both SCC and VC/VS targets have been extensively used with mixed results. While both targets can have an antidepressant effect, there are notable qualitative differences in behavioral or symptomatic responses ("activating" vs "calming")[7,8,11,20,42]. Therefore, while we expect there to be similarity in neural responses across a subset of circuits involved in mood processing, we hypothesized that there would also be differences in the frontotemporal neural substrates modulated by stimulation of the two targets.

Here, we took an advantage of a unique opportunity afforded through an ongoing clinical trial of DBS for TRD and sought to comprehensively assess the network-level effects of stimulation between two well-established targets used for DBS therapy. To evaluate the neurophysiological effects of stimulation between these two targets, we performed stimulation experiments using segmented DBS leads in the SCC and VC/VS with concurrent high-density intracranial recordings providing high spatiotemporal resolution of neural activity in participants with TRD. While surgically invasive, DBS provides substantive specificity in control in the selected anatomical targets with the ability to deliver stimulation with millisecond precision. Since we were interested in the network-level effects, we analyzed spectral power across a range of predefined frequency bands across the sampled network. Our results demonstrate overlapping effects from stimulation between the VC/VS and SCC and indicate the presence of a shared frontotemporal circuit between the SCC and VC/VS with differential effects on gamma activity depending on the target being stimulated. We also observe subject-specific differences in the response to stimulation in the VC/VS and SCC. These results lay the groundwork for a more

mechanistic understanding of the effects of DBS across implicated circuits in psychiatric disease, and better equip us to implement optimized, network-guided neuromodulation in the future.

Results

The goal of our study was to quantify prefrontotemporal network effects of intracranial stimulation delivered to two commonly used anatomical targets: the SCC and VC/VS. We obtained high-density sEEG recordings during stimulation across four steerable DBS leads implanted bilaterally in both targets in three subjects (Fig. 1). To evaluate the effect of stimulation across these targets on neural activity, we analyzed spectral power across low and high frequency bands ranging 1-100 Hz.

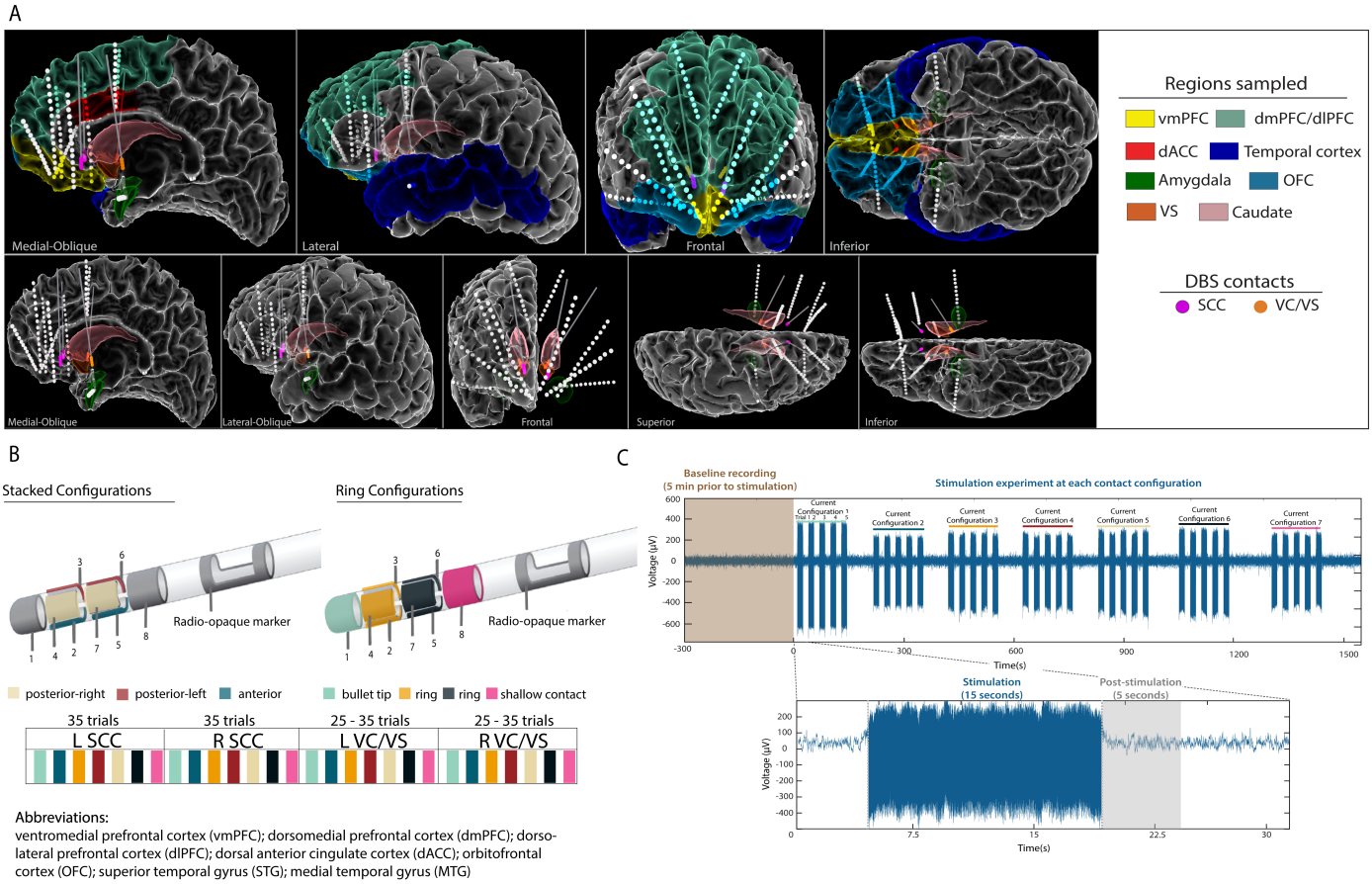

Figure 1: Experimental Approach. (A) Anatomical reconstruction showing placement of sEEG electrodes (top panel) and DBS leads (bottom panel). Colors in the legend (right) correspond to the region where electrodes were implanted. (B) Steerable DBS leads were used to deliver unilateral stimulation in the VC/VS and SCC respectively. Seven current configurations of interest were identified and tested across subjects. (C) Raw voltage signal recorded on an example sEEG contact during stimulation in the left SCC DBS lead. Subjects were systematically tested at each current configuration for fifteen seconds, with five trials per current configuration at each respective DBS lead. A five-second window following stimulation was used for subsequent analyses.

Stimulation in the VC/VS and SCC drives network-wide changes in spectral power

The extensive recording electrode coverage in our participants enabled us to assess the distributed network-level effects in neural oscillations (as measured by spectral power across predefined frequency bands) in response to stimulation across DBS leads. A representative example of the electrode coverage is shown in Fig. 2a, which illustrates the modulation of low frequency power (theta) and high frequency power (high gamma) across recording contacts in response to unilateral stimulation in Subject A. The color of each recording contact represents t-statistic values computed between post-stimulation and baseline. Stimulation of a single DBS lead in one hemisphere resulted in bilateral modulation of spectral power across frequencies (Fig. 2a).

As previous studies have shown connecting fibers and subcortical connections between the SCC and the ventral striatum (VS)[21,23], we sought to identify whether these connections may result in co-activation in any of the same networks in response to SCC or VC/VS stimulation. We examined the change in spectral power across each region of interest (ROI). We averaged power spectral density (PSD) values for each frequency band of interest for each ROI and computed a t-statistic between post-stim and baseline windows for the three subjects (see Methods) to compare the overall effect of stimulation on neural activity (Fig. 1b-d; Fig 1b-d is also color-coded by frequency band for ease in interpretation in Supplementary Fig. S2). We performed statistical analysis to evaluate significant differences between spectral power during baseline and post-stimulation and report corrected p-values in Supplementary Table S2. We found that within each subject, there were instances of unilateral VC/VS or SCC stimulation eliciting the same electrophysiological response across regions (Fig. 2b-d; p-values used to indicate distinct or overlapping responses between SCC and VC/VS are reported in Supplementary Table S5-6).

In subject A, we found that left SCC or left VC/VS stimulation drove a significant decrease in delta power in dACC relative to baseline (p-values <0.01, corrected; Supplementary Table S1). Beta power in dlPFC significantly increased following right SCC or right VC/VS stimulation (p-values <0.05, corrected; Supplementary Table S1), while alpha power in mOFC significantly increased in response to SCC stimulation in either hemisphere, or left VC/VS stimulation (p-values <0.01, corrected; Supplementary Table S1).

In subject B, we found that stimulation in the left SCC and left VC/VS led to significantly decreased beta (p-values <0.01, corrected; Supplementary Table S1) and increased low gamma activity (p-values <0.001,

corrected; Supplementary Table S1) in the dACC, as well as significantly decreased alpha (p-values <0.05, corrected; p-values reported in S2), and theta (p-values <0.001, corrected; Supplementary Table S1) activity in the dlPFC, significantly decreased low gamma power in the STG (p-values <0.05, corrected; Supplementary Table S1) and significantly increased high gamma power in the SFG (p-values <0.001, corrected; Supplementary Table S1). Stimulation in the right DBS leads for either SCC or VC/VS decreased beta activity and increased high gamma activity in the dACC while resulting in significantly increased high gamma activity in the dlPFC.

Statistically significant responses following stimulation were also observed in Subject C. Specifically, we observed that theta and alpha power was significantly increased in the dlPFC following stimulation in the left or right VC/VS (p-values<0.05, corrected; Supplementary Table S3 and S4), as well as the left SCC (p-values<0.01, corrected; Supplementary Table S1). Additionally, power in theta, alpha and high gamma was increased in the mOFC following stimulation in the left SCC (p-values<0.05, corrected; Supplementary Table S1) or left VC/VS (p-values<0.05, corrected; Supplementary Table S3), as well as right SCC or right VC/VS. Left SCC stimulation increased theta power in lOFC (p-values<0.05, corrected; Supplementary Table S1), while left VC/VS increased alpha power in lOFC (p-values<0.05, corrected; Supplementary Table S3), and right VC/VS stimulation increased both alpha and theta power in lOFC (p-values<0.01, corrected; Supplementary Table S4). A significant increase was seen in alpha power in the SFG only following left VC/VS stimulation (p-value<0.05, corrected; Supplementary Table S3).

Our results indicate broadly distributed large effects elicited from stimulation observed in neural activity in both slow and fast oscillations across the sampled network. The effects of stimulation were notably similar between the VC/VS and SCC when assessing the neural activity across spectral frequencies in the dlPFC and dACC, particularly in subjects A and B, whereas for subject C the effects elicited from stimulation between the two DBS targets were comparable across most spectral frequencies in the mOFC.

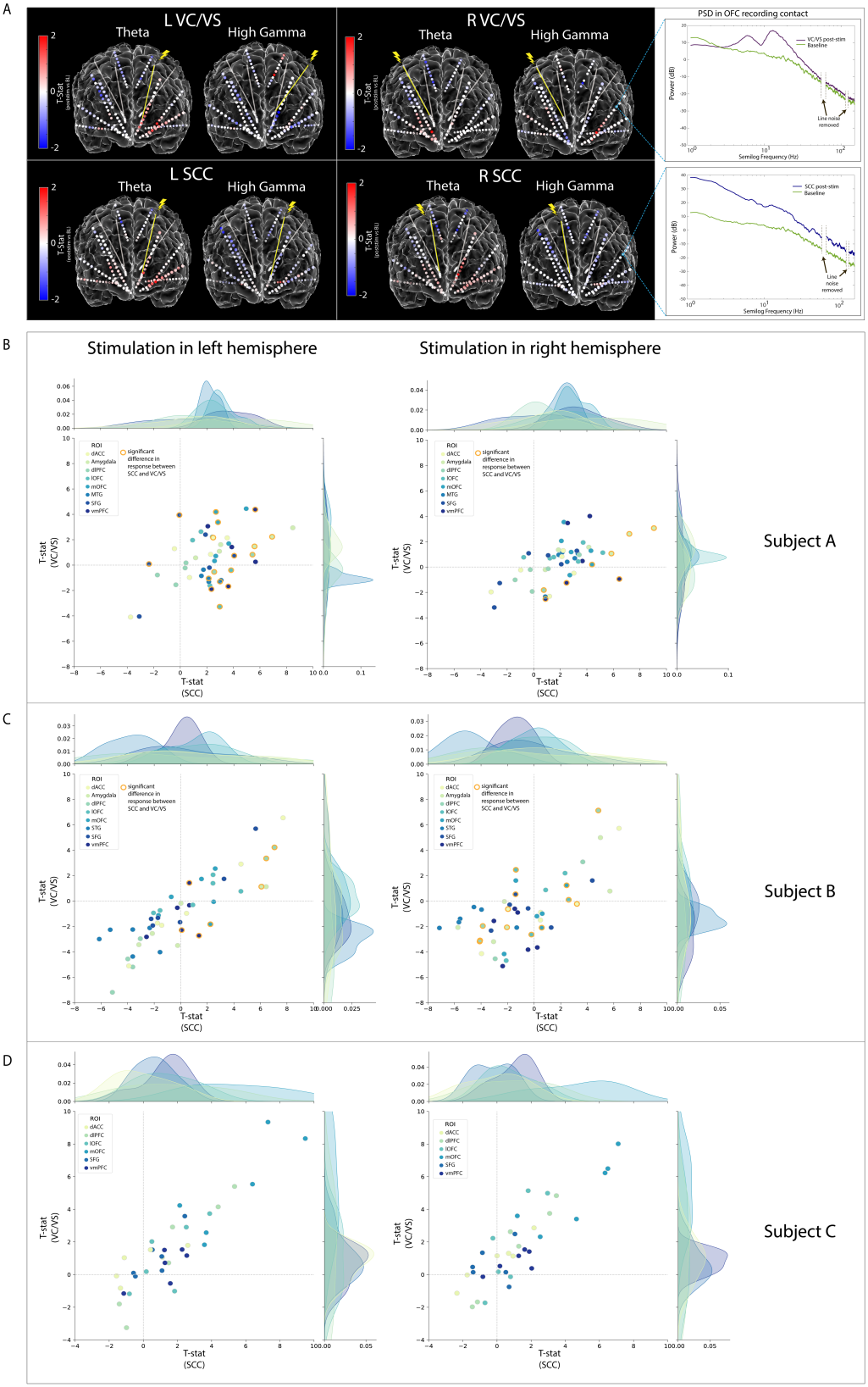

Figure 2: **Network response following stimulation in the VC/VS and SCC.** (A) Electrode diagram showing the mean power change in theta band and high gamma band following stimulation for subject A. Each contact is colored based on the t-statistic value computed between baseline and post-stimulation for each DBS lead (red indicates increase in power following stimulation and blue indicates a decrease in power following stimulation). Inset (top-right) shows log-transformed power spectra from a recording electrode in the dlPFC during baseline and post-stimulation. (B-D) Panels show t-statistic values computed between power (across six pre-defined frequency

bands) during baseline and post-stimulation for SCC(x-axis) and VC/VS (y-axis). Each data point represents the t-statistic value for a frequency band, color-coded by ROI. The plots highlight both significantly distinct (data points with gray border) and overlapping (data points without a gray border) responses between the SCC and VC/VS across neural features of interest and regions of interest.

VC/VS and SCC differentially modulate gamma-band power across prefrontal cortices and the amygdala

To characterize the differential effects of VC/VS stimulation compared to SCC stimulation, we identified neural features that were significantly different between the two targets across sampled regions. VC/VS stimulation suppressed gamma-band power, whereas SCC stimulation increased gamma-band power across the lOFC, vmPFC and amygdala, respectively, in the first two subjects. We found statistically reliable differences in gamma activity following stimulation between the two DBS targets across the lOFC (p-value<0.05, corrected; Supplementary Table S5-6), vmPFC (p-value<0.01, corrected; Supplementary Table S5-6) and amygdala (p-value<0.05, corrected; Supplementary Table S5-6), regardless of the hemisphere of stimulation (left VC/VS versus left SCC or right VC/VS versus right SCC) across Subjects A and B (Fig. 3, Supplementary Table S5-6). No statistically significant differences across these regions were observed in Subject C, which may be due to the smaller number of trials tested per DBS lead.

The opposing effects of stimulation between the two DBS targets in high frequency activity extended to the beta band as well, although this was primarily observed in Subject A. Specifically, this phenomenon in beta activity was seen in the vmPFC and amygdala, irrespective of the hemisphere of stimulation, and partially seen in the lOFC following stimulation of DBS leads in the left hemisphere (Fig. 3c, Supplementary Table S5-6).

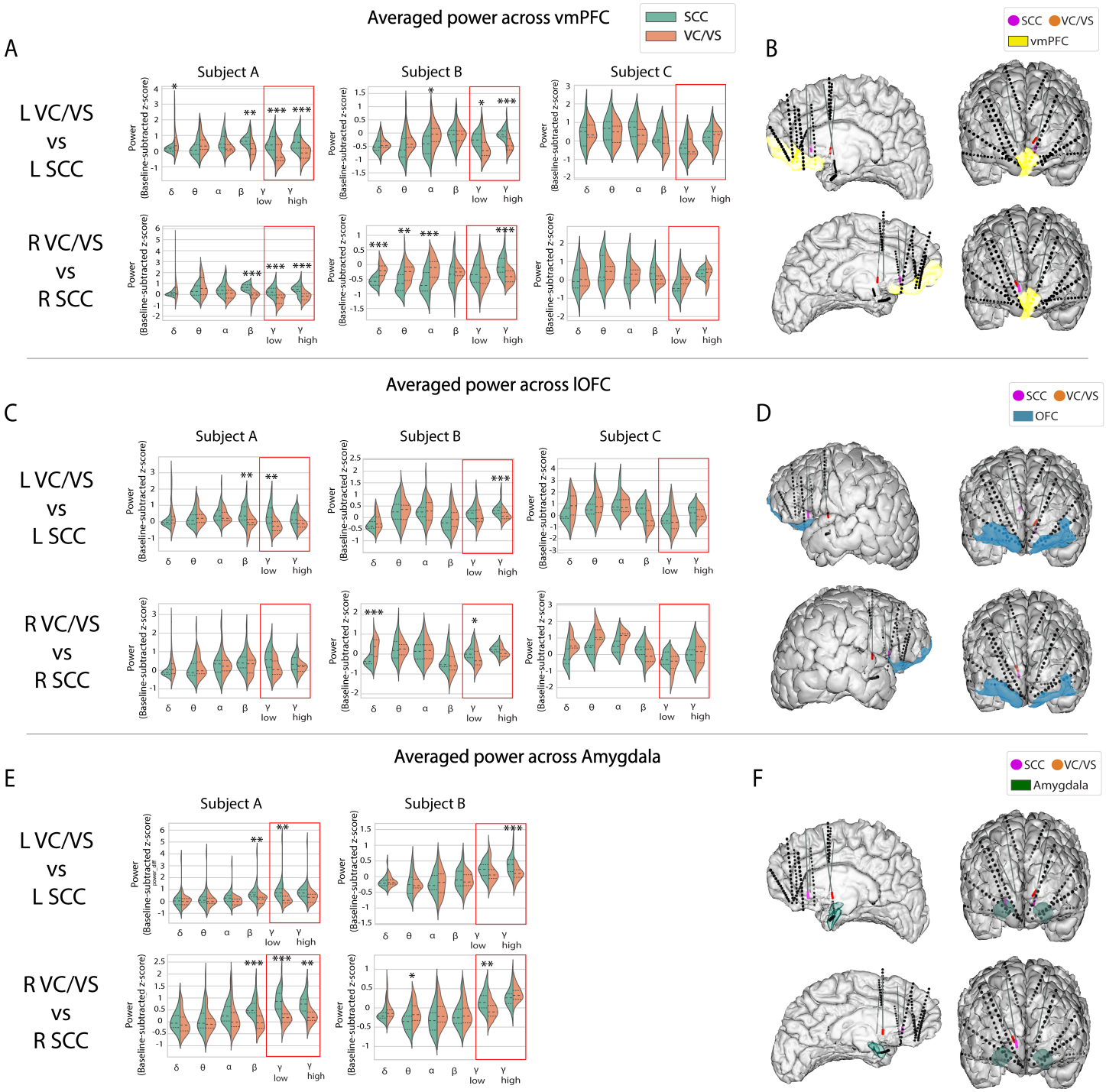

Figure 3: VC/VS stimulation suppresses gamma oscillations while SCC stimulation enhances gamma oscillations. Distribution of spectral power across all post-stimulation trials for VC/VS and SCC after z-scoring and baseline-subtraction in six pre-defined frequency bands (delta, theta, alpha, beta, low gamma, high gamma; left) with corresponding anatomical location (right) highlighted for the vmPFC (A-B), lOFC (C-D) and Amygdala (E-F).
* indicates significance where p-value <0.05, corrected; ** indicates significance where p-value<0.01, corrected; *** indicates significance, where p-value<0.001, corrected.

Brain-wide dynamics are subject-specific across frontotemporal and limbic networks

Previous studies have indicated that dysfunctional brain circuits in individuals with psychiatric disorders may be patient-specific and may need personalized treatment to achieve therapeutic efficacy[6,43]. While we observed common neural responses across the first two subjects in three regions following stimulation, we also found statistically significant differences in response to VC/VS and SCC stimulation in other regions and spectral bands specific to the individual. Fig. 4a illustrates example responses in regions sampled for each subject. A summary of neural responses that are subject-specific are shown in Fig. 4b. In Subject A, the inverse correlation between SCC and VC/VS stimulation-driven changes (increased power following SCC, decreased power following VC/VS) are observed following unilateral stimulation in the left hemisphere in low gamma power for dACC (p-value<0.05, corrected; Supplementary Table S5), alpha and beta power for dlPFC (p-value<0.01, corrected; Supplementary Table S5), delta, beta and high gamma power for SFG (p-value<0.05, corrected; Supplementary Table S5), and alpha and beta power in the MTG (p-value<0.05, corrected; Supplementary Table S5). The direction of modulation is reversed for delta and theta power in the mOFC (p-value<0.05, corrected; Supplementary Table S5), as well as high gamma in the SFG (i.e. SCC decreased power while VC/VS increased power) (p-value<0.001, corrected; Supplementary Table S5). Interestingly, stimulation of SCC and VC/VS in the right hemisphere does not elicit widespread differences in cortical response – only low gamma activity in dlPFC (p-value<0.05, corrected; Supplementary Table S6), and beta activity in mOFC (p-value<0.01, corrected; Supplementary Table S6) show increased power in response to SCC stimulation and decreased power in response to VC/VS stimulation (Fig. 4b).

Conversely, we observed in Subject B a greater prevalence of dissociable effects between VC/VS and SCC stimulation when stimulation was unilaterally delivered in the right hemisphere (Fig. 4c). When stimulated in the right hemisphere, VC/VS increased delta power while SCC suppressed delta power in the dACC (p-value<0.01, corrected; Supplementary Table S6), mOFC (p-value<0.01, corrected; Supplementary Table S6), SFG (p-value<0.05, corrected; Supplementary Table S6) and STG (p-value<0.01, corrected; Supplementary Table S6). Additionally, SCC stimulation in the right hemisphere decreased alpha, beta and low gamma power in the STG (p-value<0.05, corrected; Supplementary Table S6) relative to VC/VS stimulation. VC/VS stimulation in the right hemisphere decreased low gamma power in the mOFC while SCC increased low

gamma power (p-value<0.01, corrected; Supplementary Table S6). When performing stimulation unilaterally in the left hemisphere in Subject B, the opposing effects of VC/VS versus SCC stimulation (i.e. increase in power with SCC stimulation and decrease in power with VC/VS stimulation) were only seen in the gamma band of the dlPFC (p-value<0.001, corrected; Supplementary Table S5), and mOFC (p-value<0.001, corrected; Supplementary Table S5) responses. No statistically significant differences were seen across any frequency bands or ROIs in subject C (see Supplementary Table S5-6).

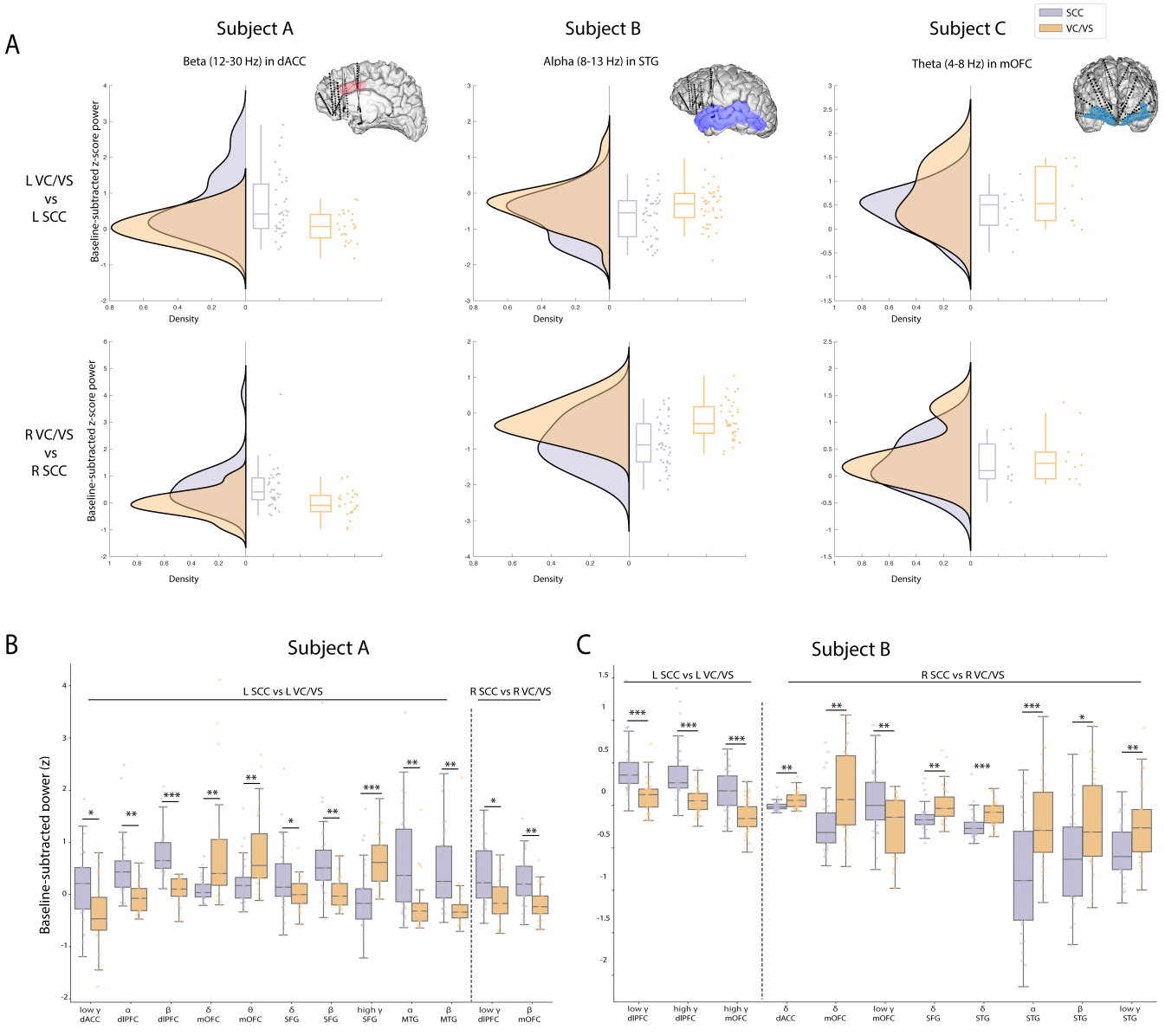

Figure 4: Significantly different neural responses to SCC vs VC/VS stimulation are subject-specific across some prefrontal and temporal networks. (A) Differences in low and high frequency band power between VC/VS and SCC stimulation are shown across three example regions in our subjects. The distribution of the z-scored baseline-subtracted power across trials is shown as a half-density plot (left) and bar plot (right; each circle indicates a single trial). (B-C) – Neural features that were statistically significant between VC/VS and SCC stimulation across all regions are shown. Subject C is not shown as there were no neural features that were significantly different between SCC and VC/VS stimulation. Error bars represent 95% confidence interval. * indicates significance where p-value <0.05, corrected; ** indicates significance where p-value<0.01, corrected; *** indicates significance, where p-value<0.001, corrected.

Current steering can drive dissociable changes in putative neural biomarkers of mood disorders

To examine whether the use of directional leads capable of current steering would allow us greater specificity in modulating neural features of interest, we evaluated spectral power for each tested contact configuration within each Cartesia™ DBS lead. Our analysis focused on neural features previously identified as putative biomarkers of depressive symptoms or shown to be involved in negative mood states. Our first feature of interest was theta-band power in the lateral OFC, which has been previously shown to be a predictor of mood severity[44] and involved in emotional processing[45]. We observed that stimulation across different contact configurations in the left or right VC/VS DBS lead differentially decreased or increased theta power in the lOFC in subject A (p-value<0.05, uncorrected; Fig. 5a and Supplementary Table S7). For example, across the left VC/VS DBS lead, stacked configurations (electrode 2-5, 3-6 and 4-7) demonstrated similar effects in modulation of theta power, while the ring configurations (electrode 1 and electrode 8) modulated power in opposite directions (stimulation of electrode 1 led to a decrease in spectral power while stimulation of electrode 8 led to an increase in power). More broadly, there were mean differences across other regions of interest between contact configurations as shown in the heatmaps (Fig. 5).

Our second feature of interest was high gamma power in the amygdala, which was recently implemented as a biomarker for a closed-loop DBS study for TRD in a single patient[10]. We observed an effect of current configuration on this neural feature following stimulation in the right SCC DBS lead, but not the left DBS lead. While there was a statistical difference (see Methods) observed following stimulation across different contact configurations on high gamma power in the amygdala (p-value<0.05, uncorrected; Fig. 5b and Supplementary Table S7) they all generally increased high gamma power to varying degrees. We replicated this analysis in Subject B for the two respective neural features (theta power in lOFC and its modulation following VC/VS stimulation, high gamma in amygdala and its modulation following SCC stimulation) but did not observe a statistically significant effect of current configuration on spectral power following stimulation in either the left or right VC/VS DBS lead (Fig. 5c), or the left SCC lead (Fig. 5d and Supplementary Table S7). Current steering did, however, distinctly modulate high gamma power in amygdala following stimulation across the right SCC DBS lead (p-value<0.05, uncorrected; Fig. 5d and Supplementary Table S7). Subject C was

excluded from this analysis because only 2 contact configurations were tested per DBS lead. These results demonstrate preliminary evidence of separable effects using current-steered DBS on putative neural biomarkers of interest for psychiatric disorders.

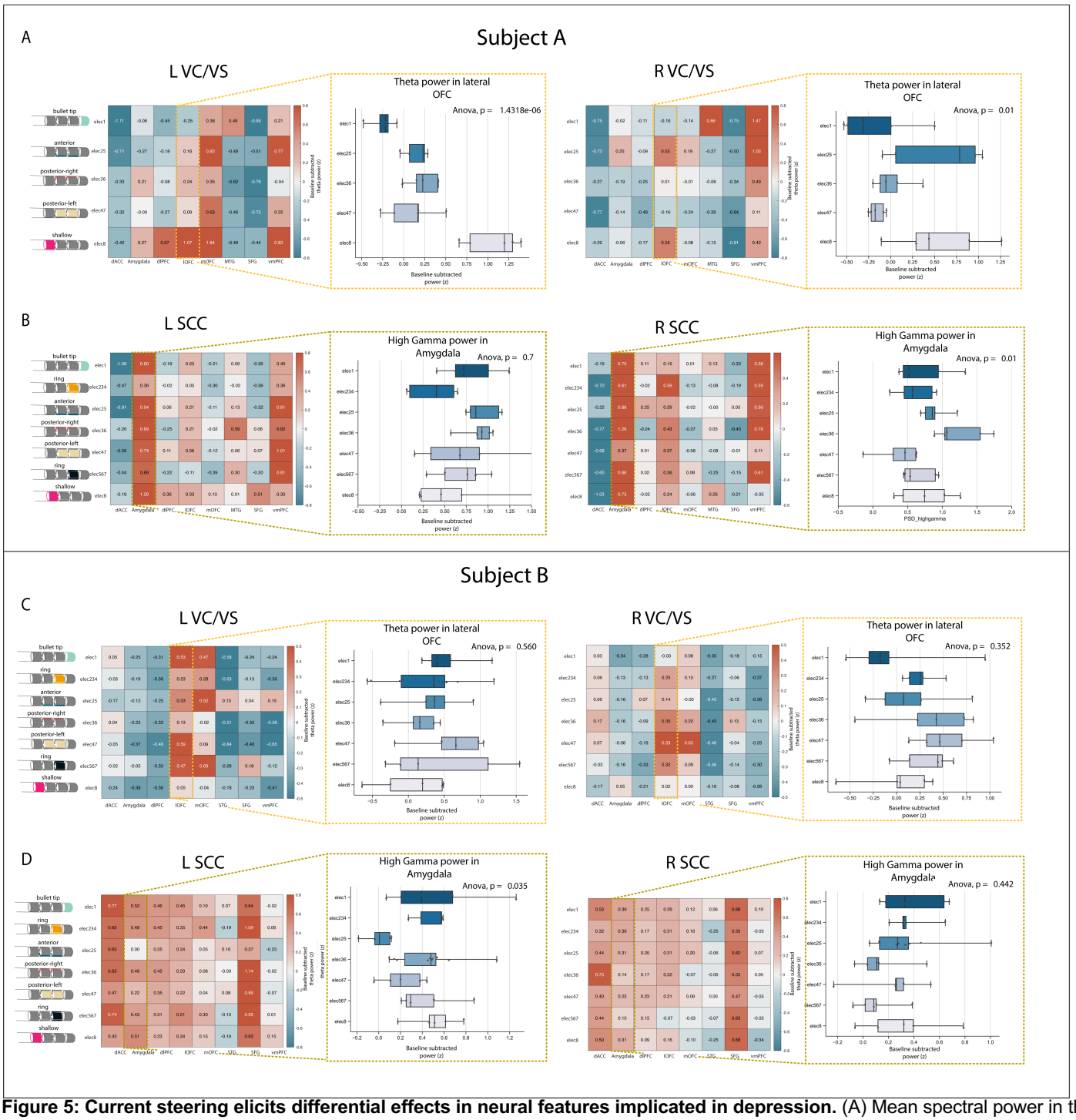

Figure 5: Current steering elicits differential effects in neural features implicated in depression. (A) Mean spectral power in theta band (left) across networks in response to current steered stimulation in the VC/VS in Subject A. Each row corresponds to a tested contact configuration across the DBS lead in the left VC/VS (left) and the right VC/VS (right). Inset shows distribution of average theta-band power across trials in the lOFC in response to stimulation in each contact configuration. (B) Mean spectral power in high gamma band across networks in response to current-steered DBS in the SCC in Subject A. Each row corresponds to a tested contact configuration in the left SCC lead (left) and the right SCC lead (right). Inset shows distribution of average high-gamma power across trials in the amygdala in response to each tested current configuration. (C) Theta power in response to current-steered VC/VS

stimulation in subject B. (D) High gamma power in amygdala in response to SCC stimulation in subject B. Error bars represent 95% confidence interval.

Discussion

Frontotemporal networks play a key role in cognitive and emotional regulation. Abnormal neural activity across nodes of frontotemporal and corticolimbic circuits manifests as dysfunctional cognitive, affective, emotional, and reward behaviors in psychiatric disorders. There exist a few anatomical regions that serve as “affective hubs” for targeted neuromodulation therapy of psychiatric disease and represent a confluence of interconnected frontotemporal brain regions. Characterizing the electrophysiological response to direct and precise manipulation of these hubs that access implicated networks will help elucidate the mechanisms of action for neuromodulation in psychiatric indications and may be critical to establishing greater clinical efficacy. Here, we show for the first time, the use of high-density intracranial recordings to distinguish the neurophysiological effects of stimulating two widely used clinical targets for neuromodulation. We illustrate that SCC stimulation drives enhancement, or an increase in gamma activity while VC/VS stimulation results in inhibition or suppression of gamma activity across a prefrontotemporal circuit, including the amygdala, lOFC and vmPFC. Previous tractography work has demonstrated that projections from the SCC and VC/VS overlap in the amygdala and medial PFC, but the anatomical trajectory and pattern of connectivity of these projections are different[24,25], as well as the sub-regions that the SCC and VC/VS project to, respectively[25]. The difference in connectivity patterns may account, at least in part, for the distinct patterns of gamma activity between the two targets. Previous studies have also observed anatomical connectivity between the SCC and the OFC, and the VC/VS and the OFC[46,47], respectively, but the differences between the trajectories of white matter tracts from the two DBS targets to the OFC, are not well understood. However, initial results from our group have shown differing effective connectivity between the SCC and VC/VS to the lOFC respectively, using diffusion tensor imaging (DTI) in participants with TRD[48]. From a electrophysiological standpoint, decreased gamma activity in the OFC following high frequency stimulation in the rodent ventral striatum[49] has been reported, supporting our findings. Surprisingly, the differential modulation in gamma power between SCC and VC/VS stimulation is seen in the lateral OFC, but not consistently seen in the medial OFC. This is consistent with previous work indicating the distinct roles of the lateral vs. medial OFC in reward and mood processing[44,50]. Additionally, although VC/VS and SCC stimulation have both been reported to improve depressive symptoms,

they have been described to modulate different dimensions of affective processing and mood: VC/VS stimulation has been reported to increase motivation and energy[20,51], while SCC stimulation has reportedly increased calmness, alertness and exteroceptive awareness[42,52]. The dissociable enhancement/suppression of gamma activity across a shared amygdala-vmPFC-lOFC circuit may be underlying the described acute behavioral reports seen elsewhere, but further work will elucidate our understanding of this phenomenon.

Important to also note are the broad range of spectral frequencies across the dACC, SFG, dlPFC and temporal gyri where differences in neural responses between SCC and VC/VS stimulation are subject-specific. (Fig. 4b-c). These significant differences in spectral power between SCC and VC/VS stimulation are additionally dependent on the hemisphere of stimulation, which is supported by previous work showing that the hemisphere of stimulation can selectively influence neural correlates of behavior[53–55].While both the SCC and VC/VS have been targeted in several DBS trials, there have been marked inconsistencies in therapeutic efficacy for both targets. For example, in the field of DBS for TRD, results from initial open-label studies for both targets have not been reproduced in larger sham-controlled trials[56,57]. This heterogeneity seen across trials may be due to inter-individual variability where DBS may have differing mechanisms of action in subjects with complex, heterogeneous symptoms and resting state activity, despite the use of identical stimulation parameters.

Neuropsychiatric disorders are posited to be network-level disorders with heterogeneous symptoms with underlying aberrant neural activity across distinct or overlapping brain networks[58], and different subsets of behavioral symptoms that cut across psychiatric disorders[59]. Failure to consider the heterogenous features of complex mental illnesses such as major depressive disorder (MDD) might partially explain why the application of the same stimulation paradigm yields very different results across a cohort of patients. The observed subject-specific stimulation responses between the VC/VS and SCC in our results suggest that increasing efforts to personalize therapy may rely on these within-subject electrophysiological signatures across networks to deliver optimized stimulation, maximize therapy and minimize side effects. Indeed, efforts utilizing subject-specific biomarkers for optimally targeted therapeutic DBS have been recently successfully demonstrated[10], and network-guided neuromodulation to treat psychiatric disorders has gained traction in recent years. An example of the latter is intermittent theta-burst TMS to treat depression, which currently utilizes resting state

functional connectivity between the neuromodulation target of interest for TMS (dlPFC) and the SCC (an extant DBS target) to determine the sub-region for stimulation targeting[5], and to predict treatment response outcomes with TMS. Future efforts incorporating behavioral measures corresponding to functional domains within mental illness, alongside electrophysiological measurements to build brain-behavior relationships in the presence of stimulation across DBS targets will help identify generalizable principles that can be potentially extended to sub-domains of MDD in the broader population[60].

The implications of our findings extend beyond the potential neurophysiological mechanisms of neuromodulation across anatomical targets. Techniques such as DTI offer immense utility in predicting therapeutic outcomes from DBS[61] and identifying optimal placement of surgical targets for DBS intervention for psychiatric indications[62]. The incorporation of electrophysiological signatures can be used to complement tractography to better characterize and validate network connectivity across brain disorders and be used as a gold standard to not only verify the optimal target, but also aid in stimulation parameter selection to target subject-specific behavioral symptoms and underlying spatiotemporal signatures of circuit dysfunction.

The use of steerable DBS leads provides an added parameter for differentially modulating implicated networks and neural biomarkers. We investigated the effect of current steering on putative biomarkers of mood across Subjects A and B and saw heterogeneity in our results between the two subjects. The clinical significance of current steered DBS is clear from its application in movement disorders[63] because of the well-characterized topographical organization of tracts around stimulation targets for Parkinson's disease[64], but the putative effects of current steering is unclear for psychiatric indications, as the topography is less well-established across these targets. The extent of the effect that directionality may have on connectivity across frontotemporal networks and the utility of steering stimulation around different arcs of the DBS lead for symptom improvement in psychiatric disorders requires further study.

Primary limitations of this study include the small sample size (N=3), and lack of randomization of stimulation conditions within or across the two DBS targets. While the electrophysiological results may be generalizable to other psychiatric or neurological disorders to some extent, our study was performed in subjects diagnosed with TRD, which may have underlying baseline activity that influenced the outcome of stimulation. Additionally, while a rigorous pipeline for optimal surgical targeting was implemented (previously

described in Sheth et al.[7]) one possible reason for inconsistent results within and across subjects is that small variations in targeting may result in modifications in the electrophysiological effects observed. As we were concerned about insufficient time for stimulation washout between trials and stimulation parameters, the baseline window used for analysis was a five-minute recording collected prior to stimulation experiments. To address possible temporal autocorrelation in the continuous baseline recording, we performed a correction procedure (described in Supplementary Fig. S3). However, neural features in specific regions (namely alpha band in dlPFC, delta and beta band in MTG in Subject A, and alpha band in STG and delta band in vmPFC and lOFC in Subject B) had a larger amount of autocorrelation during the baseline recording that could not be fully corrected with our approach, thus, results for those specific neural features must be viewed provisionally. Lastly, in the first two subjects (Subject A and B) where we tested multiple current configurations, we saw a clear effect of current steering on the neural features of interest in Subject A (Fig. 5a-b), but not subject B (Fig. 5c-d). While it is desirable to have increased control on the geometry of the stimulation field and enable differential engagement of networks and fibers passing through stimulation targets, the heterogeneity in our results suggest that more work is needed to understand both the topography surrounding/within stimulation targets and the relationship of different current-steered stimulation paradigms to electrophysiological and behavioral function.

Three main conclusions may be drawn from our study. First, we demonstrate that two canonical targets for psychiatric neuromodulation, the SCC and VC/VS, elicit network-wide neurophysiological responses across a broad range of spectral frequencies following stimulation. Second, we show that stimulation in the SCC and VC/VS drive opposite effects on gamma activity across the same frontotemporal circuit (vmPFC-amygdala-lOFC). Third, we highlight preliminary evidence of subject-specific neurophysiological responses to stimulation, and the ability to further modify these neural responses using current-steered DBS. Our findings have broad implications for the selection, optimization, and personalization of both invasive and non-invasive interventional neuromodulation therapy for psychiatric disorders with underlying dysregulated or aberrant activity across corticolimbic and frontotemporal networks.

Methods

Participant and study overview

Data for this study was collected from three subjects (37 year old Latino male, 57 year old Caucasian female, 66 year old Caucasian male) diagnosed with TRD. The subjects were enrolled in an ongoing clinical trial (NCT 03437928) for DBS for TRD. Each participant gave fully informed consent according to study sponsor guidelines, and all procedures were approved by the local institutional review board at Baylor College of Medicine IRB (H-43036) prior to participation. Subjects underwent stereotactic implantation of four DBS leads (Boston Scientific Cartesia, Marlborough, MA) and 10 temporary stereo-electroencephalography (sEEG) electrodes (PMT, Chanhassen, MN) based on pre-operative scans including patient-specific tractography. After implantation, the patients underwent a ten-day intracranial monitoring period for evaluation of brain networks involved in depression. Following the intracranial monitoring period, sEEG electrodes were removed and the four DBS leads were internalized and connected to two implanted pulse generators (IPG) (Boston Scientific Gevia, Marlborough, MA). Additional surgical details have been described previously[7].

Electrode implantation

All three participants were implanted bilaterally with segmented DBS leads in the VC/VS and the SCC, capable of current steering. The DBS leads used in our study consist of eight stimulation contacts: solid ring contacts at the deepest and shallow positions, as well as three-way segmented contacts located between the ring contacts. Seven total contact configurations of interest were identified per lead, including three stacked configurations listed as follows: (1) anterior-facing contacts 2 and 5, (2) posterior-left facing contacts 4 and 7 and (3) posterior-right facing contacts 3 and 6. The remaining four configurations tested were ring configurations listed as follows: (1) solid ring contact 1 (2) solid ring contact 8 (3) combination of segmented ring contacts 2, 3 and 4, and (4) combination of segmented ring contacts 5, 6 and 7 (Fig. 1b).

Intracranial sEEG electrodes for local field potential (LFP) recordings were implanted bilaterally across several cortical and subcortical targets based on previous work implicating their roles in mood, reward, as well as cognitive and affective processing[1,2,65,66]. Regions targeted included the dorsolateral prefrontal cortex (dlPFC),

ventromedial prefrontal cortex (vmPFC), dorsal anterior cingulate cortex (dACC), lateral and medial orbitofrontal cortex (lOFC, mOFC), superior frontal gyrus (SFG), superior and medial temporal gyri (STG, MTG) and the amygdala (Fig. 1a). While the first two subjects had coverage across the aforementioned regions, the third subject did not have sampling across the amygdala at the time of stimulation due to an early explant of the amygdala sEEG electrode. Postoperative CT scans and pre-operative MRI scans were aligned using the Functional Magnetic Resonance Imaging for the Brain Software Library's (FMRIB's) Linear Image Registration Tool (FLIRT). Electrode coordinates were manually determined from the co-registered CT in BioImage Suite and placed into native MRI space. The reconstructed cortical surface, segmented cortical and subcortical structures and electrode coordinates were visualized using the Multi-Modal Visualization Tool[67].

Electrode Stimulation and Recording

Monopolar cathodic stimulation was delivered through each DBS lead via a Blackrock CereStim R96 (Blackrock Microsystems, Salt Lake City, UT). A stimulation amplitude of 4.8 - 5 mA was delivered at the solid ring contacts, whereas for stacked or ring configurations this amplitude was split evenly among contacts to enable current steering, never exceeding 5 mA in total or at any time a charge density of 30 $\mu C/cm^2$. Stimulation was applied at 130 Hz, with a pulse width of 180 uS and interphase gap of 100 uS across all subjects. In subject A, we tested the seven identified stimulation combinations (3 stacked configurations, 4 ring configurations) for each DBS lead in the SCC, and five combinations (3 stacked configurations, 2 ring configurations) in each DBS lead in the VC/VS. In subject B, we tested all seven combinations across each of the four DBS leads. In subject C, we tested two combinations across each of the four DBS leads due to early sEEG electrode explantation. Each trial of stimulation consisted of 15 seconds of stimulation on followed by 10 seconds without stimulation (Fig. 1c). Trials were repeated 5 times per contact configuration per DBS lead seriatim, resulting in 25-35 trials per DBS lead for subject A, 35 trials per DBS lead for subject B, and 10 trials per DBS lead for subject C.

Data Acquisition and Signal Processing

Electrophysiological signals from implanted sEEG electrode contacts were recorded using a 256-channel NeuroPort Acquisition System (Blackrock Microsystems, Utah) at a sampling rate of 2 kHz, with a hardware

high pass filter applied at 0.3 Hz. Recordings from sEEG contacts were analyzed offline using custom scripts written in MATLAB (Mathworks Inc. Natick, MA) and Python. LFP signals were demeaned, decimated to 1 kHz and bandpass filtered between 1-250 Hz. A butterworth notch filter was applied to remove line noise at 60, 120 and 180 Hz, respectively. Recordings were bipolar re-referenced by subtracting the activity of adjacent electrode contact pairs. Any channels with excessive noise or without a clear neural signal were removed from the analysis.

To evaluate the response of the sampled networks before and after stimulation, we analyzed the spectral power in the 5 seconds following stimulation to avoid artifact contamination. We identified a window of 600 ms post-stimulation that was additionally excluded from analysis to avoid residual post-stimulation artifacts in the signal. The multitaper spectral estimation method was used to extract power spectral density (PSD) from the sEEG recording using the *mspectrumc.m* function from the Chronux toolbox[68]. Spectral power was then averaged within standard frequency bands (delta = 1-4 Hz, theta = 4-8 Hz, alpha = 8-12 Hz, beta = 12-30 Hz, low-gamma = 30-55 Hz, high-gamma = 65-100 Hz). The spectral power across the baseline windows and post-stimulation windows across all stimulation experiments were z-scored within subjects. Electrode contacts in gray matter located in the regions of interest were identified and pre-processed signals were then grouped (averaged) per region of interest. The location of electrode contacts in gray matter vs white matter and the labels for anatomical region of interest was verified by visual review of the MRI and CT by an expert rater (BS).

Prior to starting the stimulation experiments, 5 minutes of baseline recording was collected for each subject (Fig. 1c). To avoid temporal autocorrelation, the autocorrelation was computed for spectral power within each frequency band of interest and region of interest, across time (Supplementary Fig. S3). The number of lags *t* where the autocorrelation was at or below 0.1 and all subsequent autocorrelation values were between 0.1 and -0.1. Lag *t* was then used to generate surrogate “trials” from the baseline recording, where *t* seconds was skipped every 5 seconds. The resulting 5-second trials were used for analysis to compare against the post-stimulation windows during the stimulation experiments (additional details in Supplementary Fig. S3).

Statistical Analysis

To test the difference between pre- (baseline) and post-stimulation, non-parametric permutation testing was performed using custom scripts written in MATLAB. Data labels from post-stimulation and baseline windows were randomly shuffled, and then the absolute value of the t-statistic for a two-sample, pooled variance, t-test was computed for each pair of shuffled data. This procedure was repeated 1000 times. We used a single-step maxT procedure to correct for multiple tests[69,70], namely, each absolute t-statistic was compared to the distribution (over permutations) of the maximal absolute t-statistic across all regions of interest and frequency bands of interest in order to obtain corrected p-values that control the familywise error rate (corrected p-values reported in Supplementary Table S1).

To test the difference between PSD changes across the network following unilateral VC/VS stimulation versus SCC stimulation, we subtracted the z-scored baseline data from the z-scored post-stimulation data for each DBS lead, and compared the effect of unilateral VC/VS to unilateral SCC stimulation (i.e. left VC/VS was tested against left SCC stim and right VC/VS stim was tested against right SCC stim). Data labels for unilateral SCC stimulation and unilateral VC/VS stimulation were randomly shuffled, and then the absolute value of the t-statistic for a two-sample, pooled variance, t-test was computed for each pair of shuffled data. This procedure was repeated 1000 times. We used a single-step maxT procedure to correct for multiple tests[69,70], namely, each absolute t-statistic was compared to the distribution (over permutations) of the maximal absolute t-statistic across all regions of interest and frequency bands of interest in order to obtain corrected p-values that control the familywise error rate (corrected p-values reported in Supplementary Table S2).

To test the effect of current-steering within each DBS lead on neural responses across the sampled networks, we performed a one-way ANOVA for the regions and frequency bands of interest, namely theta power in lateral OFC and high gamma power in amygdala for SCC, (uncorrected p-values, f-statistic values and degrees of freedom reported in Supplementary Table S3). However, due to the small number of trials per current configuration per DBS lead (N = 5) we did not perform additional statistical testing.

Author Contributions

SAS and KRB initiated the study. ABA, KRB, SAS, DAB designed the experiment. ABA conceptualized analysis procedures, analyzed the data, and drafted the manuscript with support from KRB, SAS and DAB. SAS, NP, VP, WKG, SJM and KRB oversaw the organization of the clinical trial, subject recruitment, and

regulatory activities. SAS and NP performed neurosurgical procedures in the subjects' clinical trials. ABA, RKM, JA, DO, BM, AA, RG, and RAN performed data collection in the neurophysiology monitoring unit. RKM, BS, MR and KRB performed MRI analysis. ABA, SAS, and DAB wrote the manuscript, and all authors had an opportunity to review the manuscript and provide intellectual feedback.

Competing Interests Statement

SAS has consulting agreements with Boston Scientific, Neuropace, Abbott, and Zimmer Biomet. NP is a consultant for Second Sight Medical Products, Abbott Laboratories, Boston Scientific, and Sensoria Therapeutics. WKG has received donated devices from Medtronic, has consulted for Biohaven Pharmaceuticals and receives royalties from Nview, LLC. SJM is supported through the use of resources and facilities at the Michael E. Debakey VA Medical Center, Houston, Texas and receives support from The Menninger Clinic. SJM has served as a consultant to Allergan, Alkermes, Axsome Therapeutics, BioXcel Therapeutics, Clexio Biosciences, COMPASS Pathways, Eleusis, Engrail Therapeutics, Greenwich Biosciences, Intra-Cellular Therapies, Janssen, Levo Therapeutics, Perception Neurosciences, Praxis Precision Medicines, Neumora, Neurocrine, Relmada Therapeutics, Sage Therapeutics, Seelos Therapeutics, and Sunovion. He has received research support from Biohaven Pharmaceuticals, Boehringer-Ingelheim, Janssen, Merck, Sage Therapeutics, and VistaGen Therapeutics.

The remaining authors declare no competing interests.

Acknowledgments

We thank our study participants for their dedication and commitment to this study. This study was supported by the National Science Foundation Graduate Research Fellowship (ABA), National Institutes of Health grant no. F99 NS124181 (ABA), UH3 NS103549 (SAS, DAB, ABA, KRB, DO, RKM, JA, VP, BM, SJM, WKG and NP), grant no. K01 MH116364 (KRB and BM), grant no. NIH R01 MH127006 (KRB and BM), grant no. R01 274MH114854 (WKG), and the McNair Foundation (SAS).

References

1. Etkin, A., Büchel, C. & Gross, J. J. The neural bases of emotion regulation. *Nat. Rev. Neurosci.* **16**, 693–700 (2015).
2. Friedman, N. P. & Robbins, T. W. The role of prefrontal cortex in cognitive control and executive function. *Neuropsychopharmacology* 1–18 (2021).
3. Williams, L. M. Precision psychiatry: a neural circuit taxonomy for depression and anxiety. *Lancet Psychiatry* **3**, 472–480 (2016).
4. Price, J. L. & Drevets, W. C. Neurocircuitry of mood disorders. *Neuropsychopharmacology* **35**, 192–216 (2010).
5. Cole, E. J. *et al.* Stanford Neuromodulation Therapy (SNT): A Double-Blind Randomized Controlled Trial. *Am. J. Psychiatry* **179**, 132–141 (2022).
6. Grover, S., Nguyen, J. A., Viswanathan, V. & Reinhart, R. M. G. High-frequency neuromodulation improves obsessive-compulsive behavior. *Nat. Med.* **27**, 232–238 (2021).
7. Sheth, S. A. *et al.* Deep Brain Stimulation for Depression Informed by Intracranial Recordings. *Biol. Psychiatry* (2021) doi:10.1016/j.biopsych.2021.11.007.
8. Mayberg, H. S. *et al.* Deep brain stimulation for treatment-resistant depression. *Neuron* **45**, 651–660 (2005).
9. Coenen, V. A. *et al.* Superolateral medial forebrain bundle deep brain stimulation in major depression: a gateway trial. *Neuropsychopharmacology* **44**, 1224–1232 (2019).
10. Scangos, K. W. *et al.* Closed-loop neuromodulation in an individual with treatment-resistant depression. *Nat. Med.* 1–5 (2021).
11. Scangos, K. W., Makhoul, G. S., Sugrue, L. P., Chang, E. F. & Krystal, A. D. State-dependent responses to intracranial brain stimulation in a patient with depression. *Nat. Med.* (2021) doi:10.1038/s41591-020-01175-8.
12. Widge, A. S. *et al.* Deep brain stimulation of the internal capsule enhances human cognitive control and prefrontal cortex function. *Nat. Commun.* **10**, 1536 (2019).

13. Quraan, M. A. *et al.* EEG power asymmetry and functional connectivity as a marker of treatment effectiveness in DBS surgery for depression. *Neuropsychopharmacology* **39**, 1270–1281 (2014).
14. Figee, M. *et al.* Deep brain stimulation restores frontostriatal network activity in obsessive-compulsive disorder. *Nat. Neurosci.* **16**, 386–387 (2013).
15. Loh, A. *et al.* Probing responses to deep brain stimulation with functional magnetic resonance imaging. *Brain Stimul.* **15**, 683–694 (2022).
16. Fridgeirsson, E. A. *et al.* Deep brain stimulation modulates directional limbic connectivity in obsessive-compulsive disorder. *Brain* **143**, 1603–1612 (2020).
17. Elias, G. J. B. *et al.* 3T MRI of rapid brain activity changes driven by subcallosal cingulate deep brain stimulation. *Brain* **145**, 2214–2226 (2022).
18. Heldmann, M. *et al.* Deep brain stimulation of nucleus accumbens region in alcoholism affects reward processing. *PLoS One* **7**, e36572 (2012).
19. Rogers, R. D. *et al.* Distinct portions of anterior cingulate cortex and medial prefrontal cortex are activated by reward processing in separable phases of decision-making cognition. *Biol. Psychiatry* **55**, 594–602 (2004).
20. Malone, D. A., Jr *et al.* Deep brain stimulation of the ventral capsule/ventral striatum for treatment-resistant depression. *Biol. Psychiatry* **65**, 267–275 (2009).
21. Heilbronner, S. R. & Haber, S. N. Frontal cortical and subcortical projections provide a basis for segmenting the cingulum bundle: implications for neuroimaging and psychiatric disorders. *J. Neurosci.* **34**, 10041–10054 (2014).
22. Haber, S. N. Neuroanatomy of Reward: A View from the Ventral Striatum. in *Neurobiology of Sensation and Reward* (ed. Gottfried, J. A.) (CRC Press/Taylor & Francis, 2012).
23. Riva-Posse, P. *et al.* Defining critical white matter pathways mediating successful subcallosal cingulate deep brain stimulation for treatment-resistant depression. *Biol. Psychiatry* **76**, 963–969 (2014).
24. Gutman, D. A., Holtzheimer, P. E., Behrens, T. E. J., Johansen-Berg, H. & Mayberg, H. S. A tractography analysis of two deep brain stimulation white matter targets for depression. *Biol. Psychiatry* **65**, 276–282 (2009).

25. Zhu, Z. *et al.* A connectomic analysis of deep brain stimulation for treatment-resistant depression. *Brain Stimul.* **14**, 1226–1233 (2021).
26. Crowell, A. L., Riva-Posse, P., Garlow, S. J. & Mayberg, H. S. Toward an Understanding of the Neural Circuitry of Major Depressive Disorder Through the Clinical Response to Deep Brain Stimulation of Different Anatomical Targets. *Current Behavioral Neuroscience Reports* **1**, 55–63 (2014).
27. Lipsman, N. *et al.* Subcallosal cingulate deep brain stimulation for treatment-refractory anorexia nervosa: a phase 1 pilot trial. *Lancet* **381**, 1361–1370 (2013).
28. Holtzheimer, P. E. *et al.* Subcallosal cingulate deep brain stimulation for treatment-resistant unipolar and bipolar depression. *Arch. Gen. Psychiatry* **69**, 150–158 (2012).
29. Ramasubbu, R., Anderson, S., Haffenden, A., Chavda, S. & Kiss, Z. H. T. Double-blind optimization of subcallosal cingulate deep brain stimulation for treatment-resistant depression: a pilot study. *J. Psychiatry Neurosci.* **38**, 325–332 (2013).
30. Lipsman, N. *et al.* Deep brain stimulation of the subcallosal cingulate for treatment-refractory anorexia nervosa: 1 year follow-up of an open-label trial. *Lancet Psychiatry* **4**, 285–294 (2017).
31. Kashanian, A., Tsolaki, E., Pouratian, N. & Bari, A. A. Deep Brain Stimulation of the Subgenual Cingulate Cortex for the Treatment of Chronic Low Back Pain. *Neuromodulation* **25**, 202–210 (2022).
32. Greenberg, B. D. *et al.* Deep brain stimulation of the ventral internal capsule/ventral striatum for obsessive-compulsive disorder: worldwide experience. *Mol. Psychiatry* **15**, 64–79 (2008).
33. Voges, J., Müller, U., Bogerts, B., Münte, T. & Heinze, H.-J. Deep brain stimulation surgery for alcohol addiction. *World Neurosurg.* **80**, S28.e21-31 (2013).
34. Kuhn, J. *et al.* Deep brain stimulation of the nucleus accumbens and its usefulness in severe opioid addiction. *Mol. Psychiatry* **19**, 145–146 (2014).
35. Mantione, M., van de Brink, W., Schuurman, P. R. & Denys, D. Smoking cessation and weight loss after chronic deep brain stimulation of the nucleus accumbens: therapeutic and research implications: case report. *Neurosurgery* **66**, E218; discussion E218 (2010).
36. Wu, H. *et al.* Deep-brain stimulation for anorexia nervosa. *World Neurosurg.* **80**, S29.e1-10 (2013).

37. Corripio, I. *et al.* Deep brain stimulation in treatment resistant schizophrenia: A pilot randomized cross-over clinical trial. *EBioMedicine* **51**, 102568 (2020).
38. Haber, S. N. & Knutson, B. The reward circuit: linking primate anatomy and human imaging. *Neuropsychopharmacology* **35**, 4–26 (2010).
39. Hilimire, M. R. *et al.* Effects of subcallosal cingulate deep brain stimulation on negative self-bias in patients with treatment-resistant depression. *Brain Stimul.* **8**, 185–191 (2015).
40. Gotlib, I. H. *et al.* Subgenual anterior cingulate activation to valenced emotional stimuli in major depression. *Neuroreport* **16**, 1731–1734 (2005).
41. Rudebeck, P. H. *et al.* A role for primate subgenual cingulate cortex in sustaining autonomic arousal. *Proc. Natl. Acad. Sci. U. S. A.* **111**, 5391–5396 (2014).
42. Choi, K. S., Riva-Posse, P., Gross, R. E. & Mayberg, H. S. Mapping the “Depression Switch” During Intraoperative Testing of Subcallosal Cingulate Deep Brain Stimulation. *JAMA Neurol.* **72**, 1252–1260 (2015).
43. Hollunder, B. *et al.* Toward personalized medicine in connectomic deep brain stimulation. *Prog. Neurobiol.* **210**, 102211 (2022).
44. Rao, V. R. *et al.* Direct Electrical Stimulation of Lateral Orbitofrontal Cortex Acutely Improves Mood in Individuals with Symptoms of Depression. *Curr. Biol.* **28**, 3893-3902.e4 (2018).
45. Chen, W. *et al.* Altered Prefrontal Theta and Gamma Activity during an Emotional Face Processing Task in Parkinson Disease. *J. Cogn. Neurosci.* **31**, 1768–1776 (2019).
46. Haber, S. N. Corticostriatal circuitry. *Dialogues Clin. Neurosci.* **18**, 7–21 (2016).
47. Johansen-Berg, H. *et al.* Anatomical connectivity of the subgenual cingulate region targeted with deep brain stimulation for treatment-resistant depression. *Cereb. Cortex* **18**, 1374–1383 (2008).
48. Adkinson, J. A. *et al.* Imaging versus electrographic connectivity in human mood-related fronto-temporal networks. *Brain Stimul.* **15**, 554–565 (2022).
49. McCracken, C. B. & Grace, A. A. Nucleus accumbens deep brain stimulation produces region-specific alterations in local field potential oscillations and evoked responses in vivo. *J. Neurosci.* **29**, 5354–5363 (2009).

50. Cheng, W. *et al.* Medial reward and lateral non-reward orbitofrontal cortex circuits change in opposite directions in depression. *Brain* **139**, 3296–3309 (2016).
51. Gibson, W. S. *et al.* The Impact of Mirth-Inducing Ventral Striatal Deep Brain Stimulation on Functional and Effective Connectivity. *Cereb. Cortex* **27**, 2183–2194 (2017).
52. Riva-Posse, P. *et al.* Autonomic arousal elicited by subcallosal cingulate stimulation is explained by white matter connectivity. *Brain Stimul.* **12**, 743–751 (2019).
53. Smart, O. *et al.* Initial Unilateral Exposure to Deep Brain Stimulation in Treatment-Resistant Depression Patients Alters Spectral Power in the Subcallosal Cingulate. *Front. Comput. Neurosci.* **12**, 43 (2018).
54. Smith, E. E. *et al.* A brief demonstration of frontostriatal connectivity in OCD patients with intracranial electrodes. *Neuroimage* **220**, 117138 (2020).
55. Widge, A. S. *et al.* Predictors of Hypomania During Ventral Capsule/Ventral Striatum Deep Brain Stimulation. *J. Neuropsychiatry Clin. Neurosci.* **28**, 38–44 (2016).
56. Dougherty, D. D. *et al.* A Randomized Sham-Controlled Trial of Deep Brain Stimulation of the Ventral Capsule/Ventral Striatum for Chronic Treatment-Resistant Depression. *Biol. Psychiatry* **78**, 240–248 (2015).
57. Holtzheimer, P. E. *et al.* Subcallosal cingulate deep brain stimulation for treatment-resistant depression: a multisite, randomised, sham-controlled trial. *Lancet Psychiatry* **4**, 839–849 (2017).
58. Sullivan, C. R. P., Olsen, S. & Widge, A. S. Deep brain stimulation for psychiatric disorders: From focal brain targets to cognitive networks. *Neuroimage* **225**, 117515 (2020).
59. Insel, T. R. The NIMH Research Domain Criteria (RDoC) Project: precision medicine for psychiatry. *Am. J. Psychiatry* **171**, 395–397 (2014).
60. Allawala, A. *et al.* A Novel Framework for Network-Targeted Neuropsychiatric Deep Brain Stimulation. *Neurosurgery* **89**, E116–E121 (2021).
61. Clark, D. L. *et al.* Tract-based analysis of target engagement by subcallosal cingulate deep brain stimulation for treatment resistant depression. *Brain Stimul.* **13**, 1094–1101 (2020).
62. Riva-Posse, P. *et al.* A connectomic approach for subcallosal cingulate deep brain stimulation surgery: prospective targeting in treatment-resistant depression. *Mol. Psychiatry* **23**, 843–849 (2018).

63. Vitek, J. L. *et al.* Subthalamic nucleus deep brain stimulation with a multiple independent constant current-controlled device in Parkinson's disease (INTREPID): a multicentre, double-blind, randomised, sham-controlled study. *Lancet Neurol.* **19**, 491–501 (2020).
64. Vanegas-Arroyave, N. *et al.* Tractography patterns of subthalamic nucleus deep brain stimulation. *Brain* **139**, 1200–1210 (2016).
65. Knudsen, E. B. & Wallis, J. D. Closed-Loop Theta Stimulation in the Orbitofrontal Cortex Prevents Reward-Based Learning. *Neuron* **106**, 537-547.e4 (2020).
66. Miller, E. K. The prefrontal cortex and cognitive control. *Nat. Rev. Neurosci.* **1**, 59–65 (2000).
67. Felsenstein, O. *et al.* Multi-Modal Neuroimaging Analysis and Visualization Tool (MMVT). *arXiv [q-bio.NC]* (2019).
68. Bokil, H., Andrews, P., Kulkarni, J. E., Mehta, S. & Mitra, P. P. Chronux: a platform for analyzing neural signals. *J. Neurosci. Methods* **192**, 146–151 (2010).
69. Westfall, P. H. & Stanley Young, S. *Resampling-Based Multiple Testing: Examples and Methods for p-Value Adjustment*. (John Wiley & Sons, 1993).
70. Nichols, T. E. & Holmes, A. P. Nonparametric permutation tests for functional neuroimaging: a primer with examples. *Hum. Brain Mapp.* **15**, 1–25 (2002).